FEATURE EXTRACTION IN THROUGH-THE-WALL RADAR IMAGING

Christian Debes[1], *Jürgen Hahn*[1], *Abdelhak M. Zoubir* [1] *and Moeness G. Amin*[2]

[1]Signal Processing Group
Technische Universität Darmstadt
Darmstadt, Germany

[2]Center for Advanced Communications
Villanova University
Villanova, PA, USA

ABSTRACT

This paper deals with the problem of automatic target classification or Through-the-Wall radar imaging. The proposed scheme considers stationary objects in enclosed structures and works on the SAR image rather than the raw data. It comprises segmentation, feature extraction based on superquadrics, and classification. We present a recursive splitting tree to obtain optimum parameters for feature extraction. Support vector machines and nearest neighbor classifiers are then applied to successfully classify among different indoor targets. The classification methods are tested and evaluated using real data generated from synthetic aperture Through-the-Wall radar imaging experiments.

Index Terms— Through-the-Wall, radar imaging, feature extraction, superquadrics, classification

1. INTRODUCTION

Through-the-Wall Radar Imaging (TWRI) [1] is an emerging technology. It allows 'seeing' through visually opaque material, such as walls, and permits an estimation of the interior building structure and room layouts. TWRI has numerous applications in civilian, law enforcement and military sectors, making it a promising tool for e.g. searching victims and survivors in fire, earthquakes and avalanches, locating humans in a hostage crisis or detecting concealed weapons and explosives without the need for entering a building or sensing from indoor. Electromagnetic waves below the S-band are used to penetrate through building walls and illuminate the scene of interest behind. Three-dimensional TWRI images can then be obtained by using a two-dimensional sensor array and applying wideband sum-and-delay beamforming [2].

The TWRI user and operator are typically faced with the challenge of proper image interpretations. This encompasses the two tasks of detection and classification. For both tasks, the difficulty lies in the targets assuming possible and different locations and orientations in the three-dimensional space, leading to variable image statistics [3]. Further, images of the same target may change, depending on system specifications and properties as well as wide range of errors in image acquisition and formulation. Accordingly, the main aim of a practical and effective TWRI system is to perform automatic and robust target detection and classification.

Previous work [3, 4] dealing with images of target behind walls focused on automatic target detection, i.e. providing a 3D binary representation of an enclosed scene, where each voxel indicates the presence or absence of a target. There is important but preliminary work done in target classification in TWRI which focused on, e.g., exploitation of micro-Doppler to classify human gait [5] or applying principal component analysis on segmented object slices [6]. In this paper, we examine a new scheme involving segmentation, feature extraction using superquadrics, and automatic target classification. As opposed to the technique presented in [6], we aim at classifying objects irrespective of their coordinates or orientations.

Section 2 describes the experimental setup used throughout this work. Image segmentation is considered in Section 3, where we make use of the Iterated Conditional Modes (ICM) [7] algorithm. Given the segmented data, feature extraction based on superquadrics [8] is carried out in Section 4. Target classification using parameters of the superquadrics is performed in Section 5, whereas Section 6 provides conclusions.

2. EXPERIMENTAL SETUP

TWRI radar experiments were conducted at the Radar Imaging Lab at Villanova University, Philadelphia, USA. The imaged scene is depicted in Figure 1(a) and consists of a metal sphere, a metal dihedral, and a metal trihedral, mounted on high foam columns hidden behind a concrete wall. These columns were placed on a turntable made of plywood to permit changing target orientations. The experimental setup includes a synthetic aperture radar (SAR) system that is placed behind the wall, where a 57×57 element array was synthesized using a single horn antenna in motion. The scene is illuminated using a stepped-frequency continuous-wave signal in the frequency range from $0.7 - 3.1$ GHz. A typical radar B-Scan (downrange vs. crossrange cut through the 3D scene), which is obtained after background-subtraction and wideband sum-and-delay beamforming [2], is shown in Figure 1(b). At

The work by Moeness Amin is in part supported by ONR, grant no N00014-07-C-0413

(a) 3D scene of interest

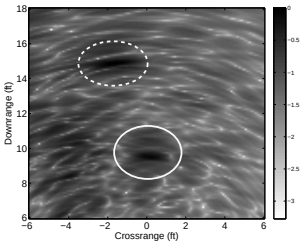

(b) Typical B-scan image

Fig. 1. Experimental setup

this specific height, only two objects can be seen in the image, namely the sphere and the dihedral, marked by solid and dashed circles. In order to obtain more data and to account for rotation factors in the classification, the scene of Figure 1(a) was illuminated from multiple views: $0, 45, 90$ and $135°$.

3. SEGMENTATION

The first part of the classification chain is data segmentation. For this purpose, the ICM algorithm [7] is applied. We choose two different classes: target and background, leading to the label set $L = \{0, 1\}$. Initialization of the segmentation is

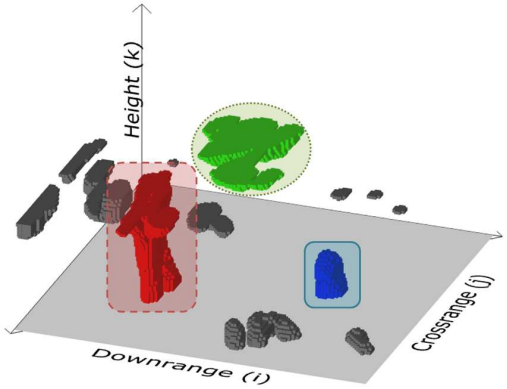

Fig. 2. Segmentation result using ICM, $\varrho = 0.01$

accomplished by Minimum Cross Entropy Thresholding [9]. Let y_n, $n = 0, ..., N-1$ denote the observed, vectorized image. Further, let x_n, $n = 0, ..., N-1$ denote the (unknown) noise-free image and $\mathcal{N}_{x_n}$ being the set representing the neighborhood of x_n. For each pixel, ICM maximizes

$$\hat{x}_n = \arg\max_{x_n} P(x_n|y_n, \mathcal{N}_{x_n}) \tag{1}$$

where $P(x_n|y_n, \mathcal{N}_{x_n})$ using a Rayleigh distribution, as typical in SAR imaging [10, 3], can be written as [10]

$$P(x_n|y_n, \mathcal{N}_{x_n}) \propto \frac{y_n}{\lambda_n^2} e^{-\frac{y_n^2}{2\lambda_n^2} + \varrho \#\{x_t \in \mathcal{N}_{x_n} | x_t = x_n\}}, \tag{2}$$

where λ_n denotes the scaling parameter of the Rayleigh distribution which can be estimated as $\hat{\lambda}_n = \sqrt{\frac{1}{2N}\sum_{n=0}^{N-1} \hat{x}_n^2}$, ϱ is the so called smoothing parameter and $\#\{\cdot\}$ denotes the cardinal number of the set. During every iteration, λ_n is first estimated, then the proportional probabilities for each possible label are computed. The new pixel value is the label that leads to a maximum of Equation (2).

For the 3D image data, a 26-neighborhood is implemented, meaning that the full dimensionality is used. The segmentation result of ICM for the experimental setup shown in Figure 1(a) is depicted in Figure 2, where $\varrho = 0.01$ is used. The object locations are indicated by dashed (dihedral), solid (sphere) and dotted (trihedral) frames.

4. FEATURE EXTRACTION

The features used for classification are obtained with superquadrics [8] which offer a simple method of describing the shape, rotation and position of 3D objects. Here, only superellipsoids are considered, with the implicit definition [8]

$$S(i,j,k) = \left(\left(\left(\frac{i}{a_i} \right)^{\frac{2}{\delta}} + \left(\frac{j}{a_j} \right)^{\frac{2}{\delta}} \right)^{\frac{\delta}{\epsilon}} + \left(\frac{k}{a_k} \right)^{\frac{2}{\epsilon}} \right)^{\epsilon} \tag{3}$$

where i, j, k are the coordinates in downrange, crossrange and height. The parameters a_i, a_j and a_k denote the superellipsoid size in each dimension and δ and ϵ are the squareness in east-west and north-south direction, respectively.

4.1. Parameter Estimation

After segmentation, we are given three dimensional binary data. Due to the implicit form of Equation (3), the parameter estimation of one superellipsoid to be fitted to one segmented object can easily be performed as follows:

For each voxel being part of the respective object shell, the distance from the surface is computed as

$$f(i,j,k,\underline{\psi}) = \sqrt{a_i a_j a_k}(S(i,j,k;\underline{\psi}) - 1) \tag{4}$$

where $\underline{\psi} = [a_i, a_j, a_k, \epsilon_1, \epsilon_2]$ and in [11] scaling by $\sqrt{a_i a_j a_k}$ is applied. The Levenberg-Marquardt method was used for nonlinear least squares minimization of $f(i,j,k,\underline{\psi})$:

$$\hat{\underline{\psi}} = \arg\min_{\underline{\psi}} \sum_i \sum_j \sum_k (f(i,j,k,\underline{\psi}))^2 \tag{5}$$

where the sum is evaluated for all (i,j,k) on the object shell. Before fitting a superellipsoid as by Equation (5), we account for rotation as well as tapering (global deformations) of the superellipsoid [11]. The estimation of the global rotation and tapering is accomplished before minimizing Equation (5) by means of the tensor product (cf. [11]). Thus, a single superellipsoid can be described by a parameter vector $\underline{\phi} = [a_i, a_j, a_k, \delta, \epsilon, \alpha_i, \alpha_j, \alpha_k, K_1, K_2]$ where α_i, α_j and α_k describe the rotation in all three dimensions and K_1 and K_2 are tapering deformations.

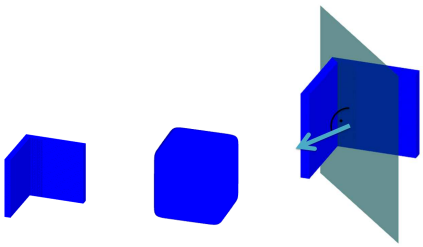

Fig. 3. Model of the L-shaped body (left), its superquadric approximation (middle) and the splitting plane (right)

4.2. Splitting objects

The procedure described above is suitable to fit only one superquadric to an object. However, objects are generally formed by a concatenation of superellipsoids. Thus, the parameter vector describing an object consisting of M superellipsoids can be written as, $\underline{\theta} = [\underline{\phi}_0, ..., \underline{\phi}_{M-1}, \underline{p}_i, \underline{p}_j, \underline{p}_k]^T$ where $\underline{\phi}_m$ describes the parameter vector of the m-th superellipsoid, as above, and $\underline{p}_i$, $\underline{p}_j$ and $\underline{p}_k$ describe the relative position of the set of superellipsoids to each other. To fit multiple superellipsoids to a segmented object, Chevalier et al. [12] suggested to perform object splitting. As such, smaller objects can be approximated by superellipsoids. This approach is followed with a few changes, adapting to the problem at hand: First, one superellipsoid is fitted to an object. Due to the large variety of possible target shapes, this might lead to a poor approximation, i.e., the difference between the segmented object and the fitted superellipsoid might exceed a critical value. In this case, the object is splitted by means of the inertia axis [12] and the superquadric parameters of each resulting object are estimated. This leads to a binary tree where for each node the respective parameter estimates and the corresponding difference error is stored. The binary tree is then scanned to obtain the minimum error.

Considering the difference error between the image data and the fitted superquadric, Chevalier et al. proposed to use the radial Euclidean distance between each voxel and the superquadric [12]. However, considering an object which can not well be approximated by a superellipsoid, such as an L-shaped object, the drawback of this approach becomes obvious. As described before, the algorithm would start to approximate the complete L, resulting in a cuboid (cf. Fig 3). Chevalier's distance measure would incorrectly lead to a low error, since the L completely fits into the shape of the cuboid.

In the following, we suggest an alternative solution. Instead of considering the distance only, the volume of the approximation and the data is taken into account. The volume of a superellipsoid is known as,

$$V_S = \frac{2}{3} a_i a_j a_k \cdot \epsilon_1 \epsilon_2 \cdot \beta\left(\frac{\epsilon_1}{2}, \frac{\epsilon_1}{2}\right) \cdot \beta\left(\epsilon_2, \frac{\epsilon_2}{2}\right)$$

where $\beta(\cdot)$ denotes the β-function. Let $V_{D,in}$ denote the volume of the data inside the fitted superellipsoid, then

$$\eta_V = \left(1 - \frac{V_{D,in}}{V_S}\right) \tag{6}$$

denotes a volume error. The ratio between the volume of the data outside the fitted superellipsoid ($V_{D,out}$) and the total data volume ($V_{D,in} + V_{D,out}$) is given by,

$$\eta_{in,out} = \left(\frac{V_{D,out}}{V_{D,in} + V_{D,out}}\right) \tag{7}$$

Eq. (6) and (7) can be combined to the total error measure,

$$\eta_e = \eta_V + \eta_{in,out} = \left(1 - \frac{V_{D,in}}{V_S}\right) + \left(\frac{V_{D,out}}{V_{D,in} + V_{D,out}}\right),$$

which can be interpreted as two penalty functions. The first part penalizes fitted superellipsoids which exceed the data size (e.g. an L-shaped object being approximated by a cube as shown in Figure 3), the second part penalizes fitted superellipsoids which are only covering small parts of the segmented object under consideration. The parameter η_e is stored for each node of the binary tree from where recursively the node (and as such the respective parameters) with the lowest error can be found. The resulting superquadric representation

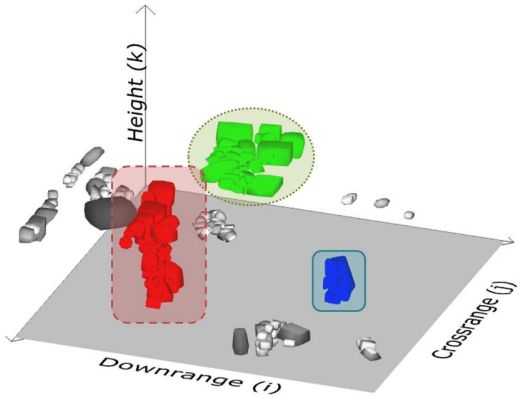

Fig. 4. Superquadric fitting of the scene

of the segmented scene depicted in Fig. 2 is shown in Fig. 4. Here, the sphere, dihedral and trihedral are represented by $9, 48$ and 35 superellipsoids, respectively.

5. CLASSIFICATION

For classification, the Nearest Neighbor classifier (NN) using the χ^2 distance is compared to Support Vector Machines (SVM) [13]. The data set consists of parameters of a dihedral, trihedral, sphere, illuminated from different vantage points as detailed in Section 2, as well and ghost targets, resulting from e.g. multipath propagation and wall effects as shown in Figure 2. In addition to all parameters resulting

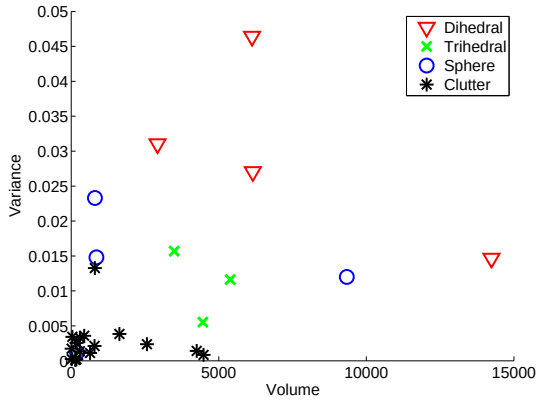

Fig. 5. Volume vs. Variance

Table 1. Confusion matrices

	NN					SVM			
class	D	T	S	C	class	D	T	S	C
D	2	1	0	1	D	2	0	0	2
T	0	0	0	4	T	0	0	0	4
S	2	0	1	2	S	1	0	0	3
C	5	4	0	8	C	0	0	0	17
Correct classification: 34.48%					Correct classification: 65.52%				

from the superquadric fitting (size, volume, squareness, tapering deformation and relative position of the concatenated superquadrics), simple statistics, namely the mean value and variance of object data are considered, motivated by the experimental results in [3], where a Gaussian distribution was suggested to model targets.

Two features, the superquadric volume and the variance are depicted for all objects in Figure 5, showing that a discrimination between objects generally is possible. For performance evaluation, classification was performed by alternately choosing one of the four datasets as a testing dataset, while the remaining three are used for training. This means that, as opposed to [6], different data sets are used for training and testing, and further, the exact orientation of the object under test is not in the database, which has made the problem more challenging. The rates of correct classification and the confusion matrices are given in Table 1 where D, S, T and C stand for dihedral, sphere, trihedral and clutter, respectively. The SVM outperforms the simple NN classifier, yielding $\approx 65\%$ correct classification. Also, one can see that the dihedral has prominent features, making classification simpler compared to either the trihedral or the sphere.

6. CONCLUSION

Automatic target classification in Through-the-Wall radar imaging was considered. The classification decision is made in the image-domain. The problems of target image segmentation, feature extraction and classification are addressed individually and applied to real data measurements. Different and discriminative target features, based on local statistics and superquadrics, which are able to represent objects behind walls and in enclosed structures, are obtained and employed in an overall classification scheme. The proposed classification scheme was applied to calibrated targets behind a concrete wall using real 3D data measurements collected by a 2D indoor scanner. We have demonstrated that when using support vector machines, desirable classification results can be achievable.

7. REFERENCES

[1] M. Amin and K. Sarabandi (Guest Editors), "Special issue on remote sensing of building interior," *IEEE Transactions on Geoscience and Remote Sensing*, vol. 47, no. 5, May 2009.

[2] F. Ahmad and M.G. Amin, "Wideband synthetic aperture imaging for urban sensing applications," *Journal of the Franklin Institute*, vol. 345, no. 6, pp. 618–639, Sept. 2008.

[3] C. Debes, M.G. Amin, and A.M. Zoubir, "Target detection in single- and multiple-view through-the-wall radar imaging," *IEEE Transactions on Geoscience and Remote Sensing*, vol. 47(5), pp. 1349 – 1361, May 2009.

[4] C. Debes, J. Riedler, M. Amin, and A. Zoubir, "Iterative target detection approach for through-the-wall radar imaging," in *IEEE International Conference on Acoustics, Speech and Signal Processing*, 2009, pp. 3061 – 3064.

[5] B. G. Mobasseri and M.G. Amin, "A time-frequency classifier for human gait recognition," in *Proceedings of the SPIE*, 2009.

[6] B. G. Mobasseri and Z. Rosenbaum, "3D classification of through-the-wall radar images using statistical object models," in *IEEE Workshop on Image Analysis and Interpretation*, 2008.

[7] J. Besag, "On the statisical analysis of dirty pictures," *Journal of the Royal Statistical Society B*, vol. 48, pp. 259–302, 1986.

[8] A.H. Barr, "Superquadrics and angle-preserving transformations," *IEEE Computer Graphics and Applications*, vol. 1, no. 1, pp. 11–23, 1981.

[9] G. Al-Osaimi and A. El-Zaart, "Minimum cross entropy thresholding for SAR images," in *Proc. of the 3rd Int. Conf. on Information and Communication Technologies*, 2008.

[10] N.D.A. Mascarenhas and A.C. Frery, "SAR image filtering with the ICM algorithm," in *Proc. of the IEEE Int. Geoscience and Remote Sensing Symposium*, 1994, vol. 4, pp. 2185–2187.

[11] F. Solina and R. Bajcsy, "Recovery of parametric models from range images: the case for superquadrics with global deformations," *IEEE Transactions on Pattern Analysis and Machine Intelligence*, vol. 12, no. 2, pp. 131–147, 1990.

[12] L. Chevalier, F. Jaillet, and A. Baskurt, "Segmentation and superquadric modeling of 3d objects," in *Int. Conf. on Computer Graphics, Visualization and Computer Vision*, 2003.

[13] T. Joachims, *Making large-Scale SVM Learning Practical. Advances in Kernel Methods - Support Vector Learning*, MIT Press, 1999.